Hindawi
Journal of Chemistry
Volume 2022, Article ID 2041512, 12 pages
https://doi.org/10.1155/2022/2041512

Research Article

Amino Acid-Doped Polyaniline Nanotubes as Efficient Adsorbent for Wastewater Treatment

Zhao Zhao, Yimin Yang, Longfei Xu, Zihan Qiu, Ziheng Wang, Yongfeng Luo, and Kun Du

Hunan Province Key Laboratory of Materials Surface and Interface Science and Technology, College of Materials Science and Engineering, Central South University of Forestry and Technology, Shaoshan South Road, No. 498, Changsha 410004, China

Correspondence should be addressed to Kun Du; dukun@csuft.edu.cn

Received 15 February 2022; Revised 4 May 2022; Accepted 13 May 2022; Published 23 May 2022

Academic Editor: Andrea Petrella

A natural amino acid-doped polyaniline nanostructure was prepared by a simple in situ chemical polymerization method in an aqueous medium. The structure and morphology of composite material were characterized by FESEM, TEM, FT-IR, and XRD. The results showed that the product possesses a large aspect ratio and a hollow tubular morphology. As-synthesized products were further applied to remove dyes and heavy metal ions from the aqueous solution, which exhibited good removal capacity toward Congo red (955.6 $mg{\cdot}g^{-1}$) and Cr(VI) (60.0 $mg{\cdot}g^{-1}$). The adsorption data for the former were found to be well described by the pseudo-first-order kinetic and Langmuir adsorption isotherm model. Thermodynamic studies show that the adsorption of Congo red by GluP is a spontaneous and endothermic process. Moreover, cyclic experiment results show that the polyaniline composites exhibited good recyclability. Therefore, these amino acid-doped polyaniline nanotubes can be expected to be an ideal candidate for the removal of organic dye and heavy metal ions from wastewater.

1. Introduction

With the rapid development of the global economic situation, the global problem of water pollution has become a serious challenge for human society. On the one hand, the increasingly frequent discharge of organically polluted wastewater during various human activities continues to pollute freshwater systems and terrestrial ecosystems. Organic contaminants are widespread in the environment, including pesticides, personal care products, pharmaceuticals, and organic dyes [1–5]. Generally, these emerging pollutants are harmful, bioaccumulating, and persistent and pose a potential threat to aquatic organisms and human beings. On the other hand, rapid industrialization led to a transitional release of heavy metals into the environment. They are usually toxic and carcinogenic and originate mainly from mining activities, petroleum refining, battery manufacture, smelting, and printing. Even more important is the fact that heavy metals can be accumulated in living organisms for the long term without degradation [5]. Therefore, more and more researchers have been looking for suitable methods to obtain high-quality drinking water free from organic pollutants and heavy metals over the past few decades.

To date, several techniques have been developed for the purification of industrial wastewater, such as biological, physical, and chemical methods. Among the different treatment strategies, physical adsorption is often regarded as one of the most economical and competitive options due to its low cost, high efficiency, and ease of operation [3–5]. Different types of adsorbents, including mesoporous silica composites, metal-organic frameworks, biomass materials, polymer-based materials, and carbon materials, have been applied for pollutant removal from industrial wastewater. However, the development of green and efficient adsorbents remains an ongoing challenge considering ease of operation, cost-effectiveness, eco-friendliness, and reusability for water treatment. Among various water treatment materials,

polymer and polymer-based adsorbents have emerged as effective and promising candidates for removing different pollutants from the environment due to their advantages such as low cost, rich active sites, durability, and easy modification. Inherently conducting polymers, such as poly (phenylenevinylene) (PPV), polyaniline (PANI), polypyrrole (PPy), and polythiophene (PTH), are a special class of synthetic polymers and are extensively studied due to their tunable electrooptic properties and mechanical properties via bearing functional groups of the conjugated chains. As a representative conducting polymer, PANI has been widely explored for diverse applications, including separation, catalysis, sensing, thermoelectric generator, and corrosion protection [6–8]. Meanwhile, PANI is currently one of the most promising adsorbent materials due to its low price, easy synthesis, environmental friendliness, and unique doping/dedoping property [9]. Typically, the molecular structure of polyaniline contains large amounts of amine and imine functional groups, which enable them to interact with various organic/inorganic pollutants present in wastewater. Nonetheless, the adsorption capacity can be limited due to the poor porosity of pure PANI nanomaterials. Further preparation of polyaniline-based adsorbent materials with porous structures (e.g., nanotubes) by simple solutions is therefore particularly important for the continued promotion of efficient wastewater treatment.

Recently, Rana et al. prepared different polyaniline nanostructures with aromatic dopant acids via a facile chemical polymerization in the presence of ammonium persulfate. Results show that the symmetrical positioning of carboxyl groups plays an important role in the formation of polyaniline nanotubes [10]. Inspired by this strategy, we have prepared polyaniline nanotube composites using amino acids as dopant acids for the removal of toxic pollutants from water environment. As an acidic amino acid, glutamate (with two carboxyl groups) is a kind of desirable dopant for regulating the morphology of polyaniline. In this work, therefore, natural glutamic acid was used as a dopant for fabricating polyaniline-based adsorbent with hollow tubular morphology in an aqueous solution at a low temperature. As-synthesized GluP nanotubes were further employed to remove organic dyes (Congo red, methyl orange, indigo carmine, orange G, and crystal violet) and heavy metal ions (Cr^{6+}, Pb^{2+}, and Ni^{2+}) from the aqueous solution. The effects of adsorbent dose, contact time, pH value, and the initial dye concentration were investigated. Meanwhile, adsorption kinetic, isotherm, and thermodynamics of GluP were also studied using Congo red as a model dye molecule. Importantly, the prepared material exhibited a good cycle performance in batch experiments.

2. Experimental

2.1. Materials. Glutamic acid (Glu) and ammonium persulfate (APS) were purchased from Sigma Chemistry (Shanghai, China). Aniline, $K_2Cr_2O_7$, $Pb(NO_3)_2$, and $Ni(NO_3)_2{\cdot}6H_2O$ were obtained from Energy Chemical (Shanghai, China). Dyes used, including Congo red (CR), methyl orange (MO), indigo carmine (IC), orange G (OG), and crystal violet (CV), were purchased from Innochem (Shanghai, China). All chemicals were used as received without further treatment. Deionized water was used for solution preparation throughout the work.

2.2. Preparation of Amino Acid-Doped Polyaniline Nanotubes. In a typical reaction, the glutamic acid powder (0.35 mmol) was dissolved in 15 mL of water with continuous stirring at room temperature. Then, the solution of aniline (100 μL, 1.1 mmol) was added and stirred vigorously for 1 hour before being placed in a refrigerator freezer for 30 minutes. After the temperature of the mixtures was reduced to 4°C, the APS (1.1 mmol) aqueous was added dropwise without stirring, and the color of the solution slowly turned from yellow to brown. Eventually, a dark green precipitate was formed after standing for another 24 hours at 4°C. The pellet was washed with water and methanol several times to wash out the oligomers and excess APS from the reaction mixtures. Finally, the product was obtained by vacuum drying at 60°C overnight, named GluP. The same sample without adding amino acid was used as a control (PANI), and the preparation process was similar to the procedure described above.

2.3. Characterization. The morphology and structure of the products were characterized by using field emission scanning electron microscopy (FE-SEM, Zeiss Ultra 55, Germany) and Transmission Electron Microscopy (TEM, HT7800, Hitachi, Japan). X-ray powder diffraction (XRD) patterns were recorded using an XRD diffractometer (Bruker, D8 ADVANCE) at a scan rate of 4 min^{-1} and equipped with Cu Kα radiation ($\lambda = 0.15406$ nm) at room temperature in the 2θ range of 10–40°. The surface structure and functional groups of the samples were determined by the Fourier-transform infrared (FT-IR) spectroscopy (Shimadzu, FT-IR-8400S) with the KBr disk method.

2.4. Adsorption Investigation. Typically, the adsorption of the dyes studies was performed with the batch mode in glass vials. An equal amount of adsorbents was added to the reaction mixture with known concentrations of dyes or metal ions and gently stirred continually. Then, an aliquot of the reaction solution was taken out at an appropriate time interval and separated via centrifugation at 12000 rpm for 1 min. The concentration of dyes was monitored by a UV-Vis spectrometer according to the maximum wavelength (λ_{max} 611, 588, 478, 499, and 464 nm for IC, CV, OG, CR, and MO). The metal ion concentration was measured by inductively coupled plasma-optical emission spectroscopy (ICP-OES). The effects of experimental variables affecting adsorption, including the adsorbent dosage, pH value, and the initial dye concentration, were investigated. Besides, the recycling performance of GluP composites was also studied. For the adsorption kinetic studies, 5 mg of amino acid-doped polyaniline nanocomposites was added to 10 mL of dye solution to initiate the reaction, and the pH was fixed at neutral. The adsorption capacity, q_t, and removal efficiency,

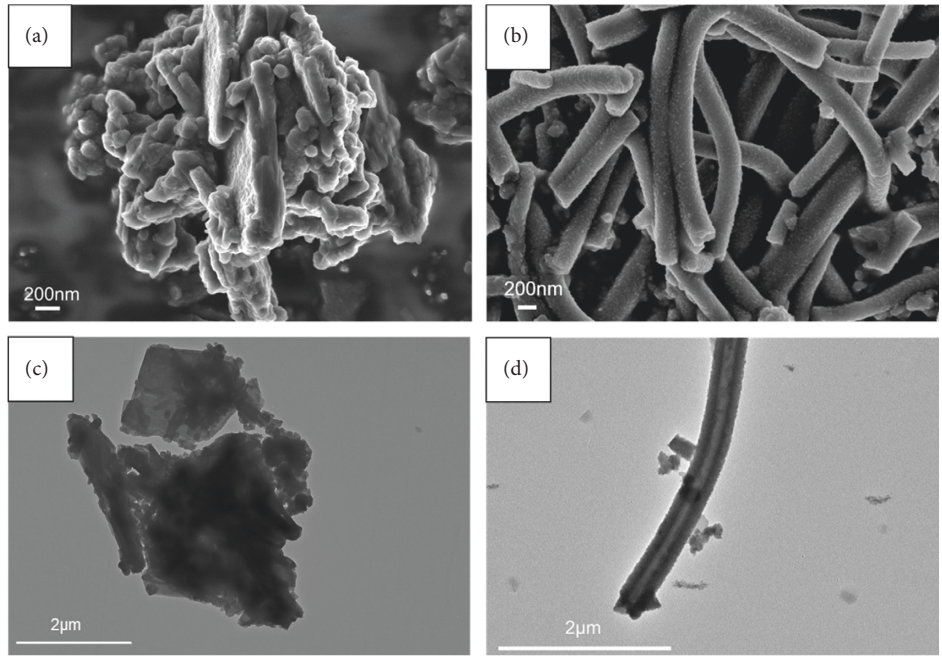

Figure 1: FESEM and TEM images of PANI (a, c) and GluP (b, d), respectively.

$R\%$, were calculated based on equations (1) and (2), respectively.

$$q_t = \frac{(C_0 - C_t)V}{m}, \quad (1)$$

$$R\% = \frac{(C_0 - C_t)}{C_0} \times 100, \quad (2)$$

where "C_0" and "C_t" are the concentration (mg/L) of dye solution at the time "0" and "t," respectively, "V" is for the total volume of reaction solution (L), and "m" is the mass of adsorbents (g) [3].

3. Results and Discussion

3.1. Characterization of PANI and GluP. GluP nanocomposites were obtained by simply mixing glutamic acid with aniline monomer reaction solution under low-temperature conditions. As a comparison, undoped PANI was also prepared under the same conditions. SEM and TEM images of PANI and GluP products are shown in Figure 1.

As shown in Figures 1(a) and 1(c), the morphology of undoped polyaniline (PANI) exhibited inhomogeneous spherical particles with serious agglomeration. This phenomenon is consistent with previously reported results that polyaniline tends to aggregate during the polymerization reaction. In the presence of glutamic acid, the product of aniline oxidation was mainly composed of one-dimensional linear nanotubes with a diameter of ~200 nm (Figures 1(b) and 1(d)). Compared with nondoped PANI, the amino acid-doped GluP with a hollow tubular structure and a large aspect ratio may be beneficial in increasing its specific surface area, thereby affecting the adsorption performance. As can be seen, the EDS spectra showed that the polyaniline

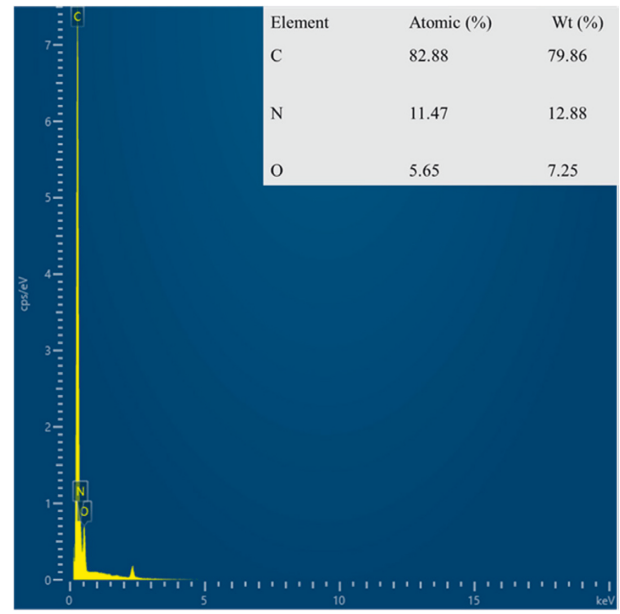

Figure 2: EDS spectra and element content analysis table of GluP composites.

tubes were composed of carbon, nitrogen, and oxygen elements (Figure 2), where the oxygen element (7.25%) may be derived from the carboxyl groups of doped glutamic acid.

Fourier-transform infrared (FT-IR) spectra of polyaniline-based adsorbents in the doped and undoped states are shown in Figure 3(a). As can be seen, the different adsorbents have similar adsorption band profiles in the infrared spectrum over the wavelength range of 400–4000 cm^{-1}. The typical stretching vibration bands of polyaniline are observed at 3443, 1581, 1501, 1299, 1148, and 823 cm^{-1} [11]. The broad band in the spectra of the samples at around 3443cm^{-1} was attributed to the stretching

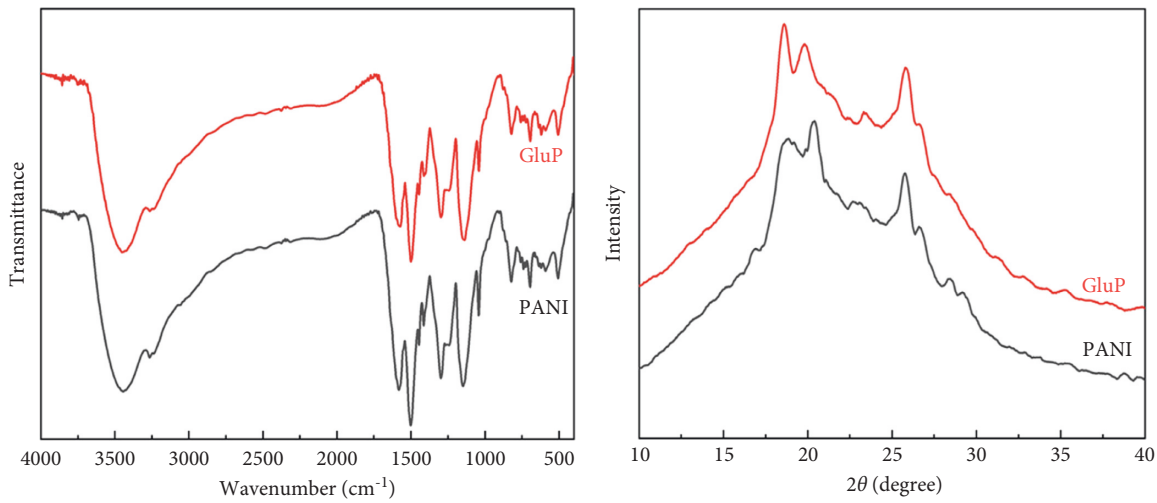

Figure 3: FT-IR spectra (a) and XRD patterns (b) of PANI and GluP, respectively.

vibration of N-H bond for polyaniline molecular chains. Peaks at 1581 and 1501 cm^{-1} can correspond to the stretching vibration of the C=C bond in the quinoid and benzenoid rings. The characteristic stretching bands at 1299 cm^{-1} for the C-N bond were associated with the secondary aromatic amine [10–13]. Moreover, the absorption bands at 1148 cm^{-1} and 823 cm^{-1} correspond to the C-H vibration of aromatic in-plane and aromatic out-of-plane deformation, respectively [14, 15]. Figure 3(b) shows the powder X-ray diffraction (XRD) patterns of PANI and GluP. Similarly, there is no obvious change in the XRD spectrum from each other, which indicates that the crystal structure had not been significantly altered after doping amino acids. All samples exhibited three main broad diffraction peaks at $2\theta \approx 18^{\circ}$, 20.4°, and 25.8°, assigned to (004), (100), and (110) planes of polyaniline. The latter two peaks correspond to the periodicity in parallel and perpendicular directions to the polymer chain of polyaniline, respectively [16, 17]. Meanwhile, the broad diffraction peak of the two samples demonstrates its poor crystallinity.

3.2. Adsorption Results. At first, Congo red (CR) was selected as a model dye molecule to explore the adsorption performance of PANI and GluP. Compared to the adsorption capacity of undoped PANI, glutamic acid-doped GluP has shown higher dye adsorption capacity as shown in Figure 4(a). According to the SEM and TEM images, this result could be explained by the morphological difference between the two types of absorbent material. For doped GluP, the tubular structure with a large aspect ratio provides more adsorption sites for enhancing the adsorption capacity. To obtain the optimal adsorption capacity between the amount of adsorbent and dye, the concentration of adsorbent (GluP) was changed, while the dye concentration (CR) was kept constant. Results of the UV-Vis absorption spectrum after treatment with different concentrations of adsorbent are presented in Figure 4(b). It is observed that the characteristic UV-Vis absorption of the CR dyes ($\lambda_{max} = 499$ nm) in the reaction system gradually decreased and then somewhat increased as the amount of adsorbent increased. Compared with a lower adsorbent concentration, the excess adsorption sites will not be fully utilized at a higher adsorbent dosage [18, 19]. Meanwhile, the background absorbance of samples was slightly increased beyond a certain concentration of adsorbent 0.25 $g{\cdot}L^{-1}$. This may be caused by oligomers of polyaniline in the supernatant after centrifugation. Overall, with the increase of the dosage of GluP, the percentage removal for CR was also increased over a range of concentrations. Maximum adsorption capacities and removal efficiencies are 111.3 $mg{\cdot}g^{-1}$ and 92.8%, respectively. And 0.25 $g{\cdot}L^{-1}$ was chosen as the fixed dose of GluP for subsequent experiments.

Normally, industrial effluents contain a variety of toxic dyes. To further test the adsorption performance in a broad sense of GluP adsorbent, more dyes were selected for adsorption studies, namely, Congo red (CR), methyl orange (MO), indigo carmine (IC), orange yellow G (OG), and crystalline violet (CV), whose structures are shown in Figure 5.

The adsorption capacity for different dyes has been monitored with different contact times by UV-Vis spectroscopy (Figures 6(a)–6(e)). Figure 6(f) shows the instantaneous adsorption capacity with different contact times calculated by equation (1) for five model dye molecules. The results show that the adsorption efficiency is influenced by the properties of the dye molecule, including the intrinsic charge nature and chemical structure, and the adsorption capacity of anionic dyes is better than that of the cationic type. Among different dye molecules, CR has shown higher uptake efficiency. It is well known that the hydrophobic and electrostatic interactions play a significant role in dye adsorption, while Congo red is an anionic dye with two sulphonic acid groups, two naphthalene rings, and a biphenyl structure in the chemical constitution. This is probably the main reason for its high removal efficiency compared with other dye molecules. In contrast, CV is a cationic dye that has the same positive charge as the polyaniline chain (emeraldine salts). Therefore, it produces the lowest rate of uptake among all dye molecules due to the electrostatic

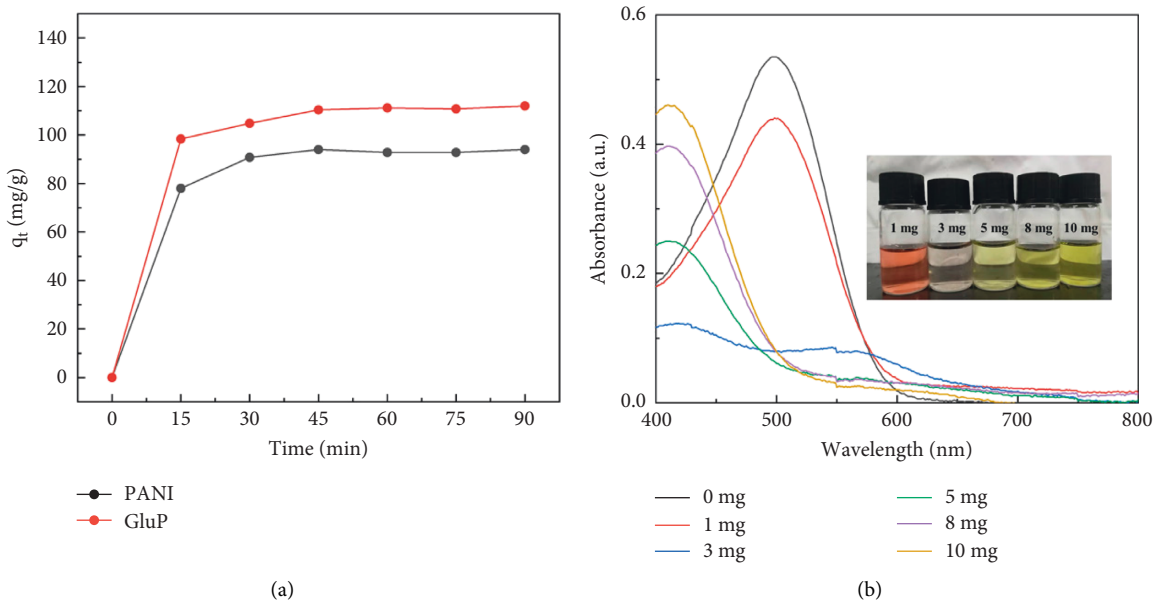

FIGURE 4: (a) Adsorption capacity of PANI and GluP at room temperature for CR (0.25 g·L^{-1} absorbent, 30 mg·L^{-1} dye, pH = 7). (b) Ultraviolet-visible spectra of CR with different adsorbent doses at a fixed dye concentration for 3 h (30 mg·L^{-1} dye, 25°C, pH = 7).

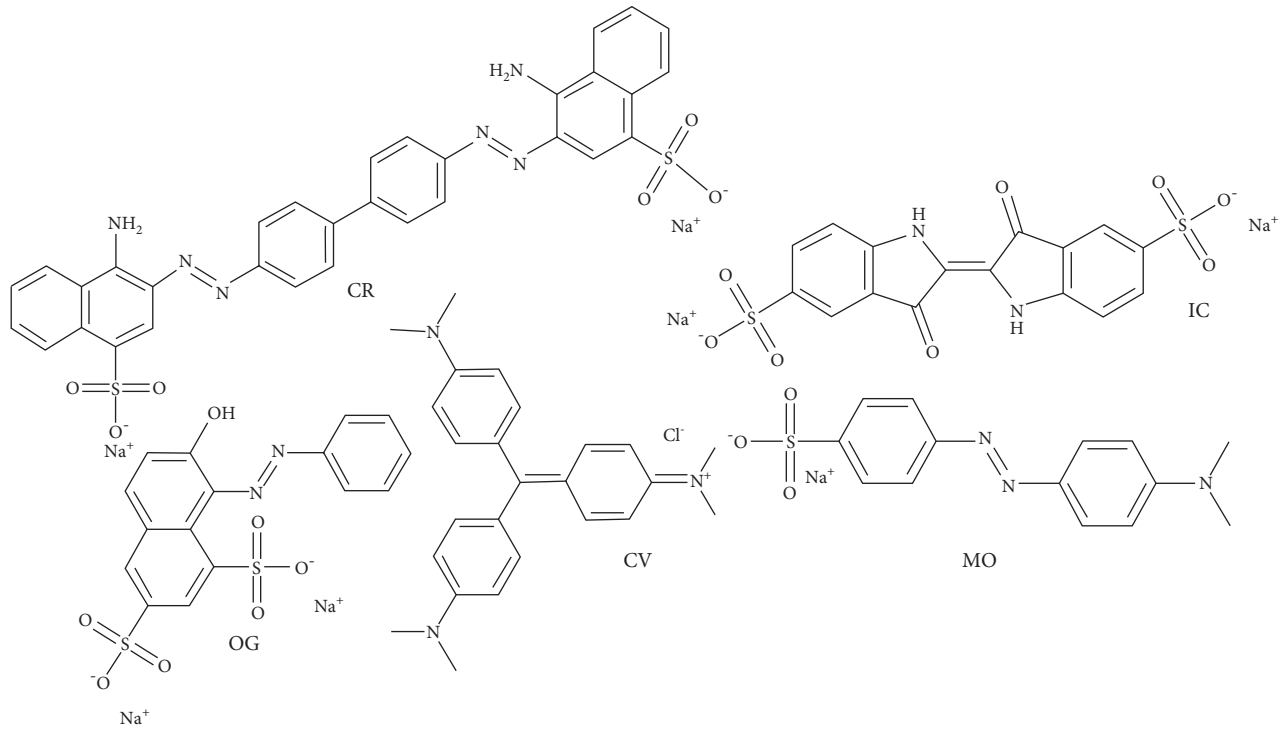

FIGURE 5: Chemical structure of different dyes (CR, MO, IC, OG, and CV).

repulsion between positive charges. Although OG, IC, and MO are anionic molecules, the MO dye has only one negative charge (sulfonic acid group) in comparison with the first two (OG and IC). At the same time, OG and IC with two sulfonic acid groups have comparable dye adsorption efficiency. On the whole, the approximate order of dye adsorption capacity is as follows: CR > OG ≥ IC > MO > CV, and the results are summarized in Table 1.

To improve the adsorption performance of adsorbent GluP for dye CR, two important experimental parameters, including pH value and the initial dye concentration that are relevant for this assay, were also studied. The effect of solution pH on adsorption capacity was first investigated by batch adsorption experiments. During the adsorption process, the environmental pH has a direct impact on the surface charge of the adsorbent and the adsorbate [19]. As

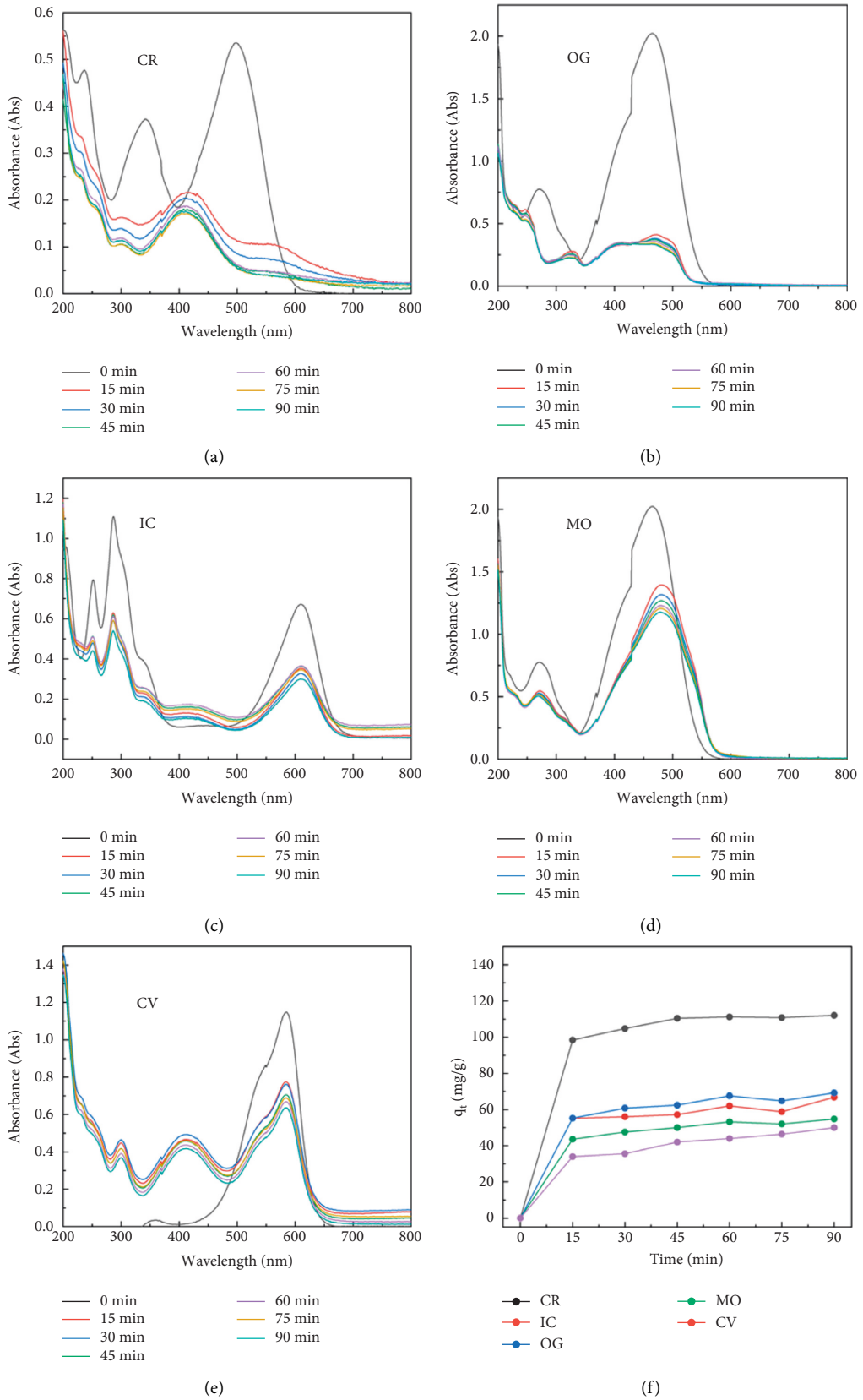

Figure 6: UV-Vis spectra of GluP adsorbent dispersed in aqueous solution collected at different time intervals, including (a) CR, (b) OG, (c) IC, (d) MO, and (e) CV. (f) The different adsorption capacity for five types of dye with GluP adsorbent at room temperature and pH 7 ($0.25\,g{\cdot}L^{-1}$ absorbent, $30\,mg{\cdot}L^{-1}$ dye).

Table 1: Adsorption efficiency for different dyes.

Dye	λ_{max} (nm)	Dye nature	Adsorption (mg/g)
CR	499	Anionic	112.0
OG	478	Anionic	69.2
IC	609	Anionic	66.8
MO	464	Anionic	54.8
CV	588	Cationic	50.0

shown in Figure 7(a), dye removal slightly elevated at pH values ranging from 3 to 5, followed by a rapid decrease in the pH range from 5 to 13. It is observed that the maximum adsorption capacity (about 117.0 $mg{\cdot}g^{-1}$) is reached under a weakly acidic medium (pH 5). With the pH switch from neutral (pH 7) to alkaline (pH 13), the adsorption capacity drops sharply to zero. This indicates that electrostatic attraction and repulsion dominate the interaction between the adsorbent and adsorbent at pH 5 and pH 13, respectively. It is well known that Congo red is a typical anionic diazo dye (pKa 4.5) with two sulfonate functional groups, while the polyaniline is positively charged when the pH value is lower than 10 as its isoelectric point is as high as 10 [20]. At lower ambient pH (pH 3), therefore, the decrease in dye adsorption is likely due to the electrostatic repulsion between adsorbate and adsorbent, both positively charged. As the pH increases, the electrostatic attraction is the main force for the adsorption of dye in the solution (pH 5). When the pH of the reaction solution exceeds the isoelectric point of GluP composites, the adsorbents become negatively charged and cause a decrease in dye adsorption capacity, especially under strongly alkaline conditions (pH 13). This also means that the dye molecules can be eluted, and the adsorbent can be regenerated at a high pH value. Besides, previous studies have also found that the zwitterionic dye molecules tend to aggregate under alkaline conditions, thereby further hindering the adsorption of dye.

Figure 7(b) plots the curve of adsorption capacity at different initial dye concentrations. It is evident that the removal efficiency increases gradually with increasing initial dye concentration in the range of 10–100 $mg{\cdot}L^{-1}$. When the dye concentration is further increased to 200 $mg{\cdot}L^{-1}$, the adsorption capacity of the adsorbent does not increase any further. The reason for this is that there are sufficient adsorption sites on the surface of the GluP adsorbent at lower initial concentrations, and as the concentration of the added dye increases, the adsorption sites are gradually saturated. That can also be explained by an increase in the adsorbate to adsorbent ratio [18]. Previous studies have found that the initial dye concentration is the main driver of mass transfer from the solution to the adsorbent [21]. With higher initial dye concentrations, the driving force for adsorption is greater, resulting in a stronger affinity of dye molecules to the adsorbent surface. At higher dye concentrations, the decrease in CR adsorption suggested that GluP may be approaching the saturation limit of adsorption [22]. On the other hand, the conductive state of polyaniline (emeraldine salt) contains a considerable quantity of amine and imine functional groups and interacts with some metal ions. Based on this consideration, GluP has been further studied for the removal of heavy metal ions (Cr^{6+}, Pb^{2+}, and Ni^{2+}) from aqueous solutions (Figure 7(c)). It can be seen that the adsorption capacity for Cr^{6+} is 60.0 $mg{\cdot}g^{-1}$ with a removal efficiency of 100%. For Pb^{2+} and Ni^{2+}, the adsorption capacities are about 40 $mg{\cdot}g^{-1}$ with removal efficiencies of around 67% under identical conditions. This result also implies that the GluP has a good adsorption capacity for hexavalent chromium.

3.3. Adsorption Behavior of GluP. To evaluate the possible mechanisms of adsorption, the adsorption kinetics of CR onto GluP were fitted by the pseudo-first-order (PFO) and pseudo-second-order models (PFO), as shown in equations (3) and (4), respectively.

$$q_t = q_e\left(1 - e^{-k_1 t}\right), \tag{3}$$

$$q_t = \frac{k_2 q_e^2 t}{1 + k_2 q_e t}, \tag{4}$$

where q_t and q_e are the adsorption capacity ($mg{\cdot}g^{-1}$) at time t (min) and equilibrium and k_1 (min^{-1}) and k_2 ($g\,mg^{-1}{\cdot}min^{-1}$) are the rate constants of PFO and PSO, respectively. Figure 8(a) illustrates the plots of q_t versus t for PFO and PSO models. The equilibrium adsorption capacity, rate constant, and correlation coefficients are determined by corresponding kinetic models, and the results are presented in Table 2. According to the results, it is clearly demonstrated that this adsorption process fitted well with both pseudo-first-order and pseudo-second-order models, while the theoretical q_e value (110.4 $mg{\cdot}g^{-1}$) calculated by the PFO model agrees better with the experimental data (112.0 $mg{\cdot}g^{-1}$) compared with the PSO model (115.4 $mg{\cdot}g^{-1}$). Therefore, the pseudo-first-order model is more suitable for describing the adsorption kinetic behavior of GluP on dye CR [18, 23].

The adsorption isotherms of Congo red on GluP were obtained at a constant temperature as shown in Figure 8(b). The experimental data were fitted by two well-known adsorption isotherm models, including Langmuir and Freundlich. The Langmuir model is commonly used to describe monolayer adsorption processes at homogeneous sites of the adsorbent, and the form can be represented by equation (5), while the latter describes multilayer adsorption on a heterogeneous system and can be defined by equation (6).

$$\frac{C_e}{q_e} = \frac{1}{K_L q_m} + \frac{C_e}{q_m}, \tag{5}$$

$$q_e = K_F C_e^{1/n}, \tag{6}$$

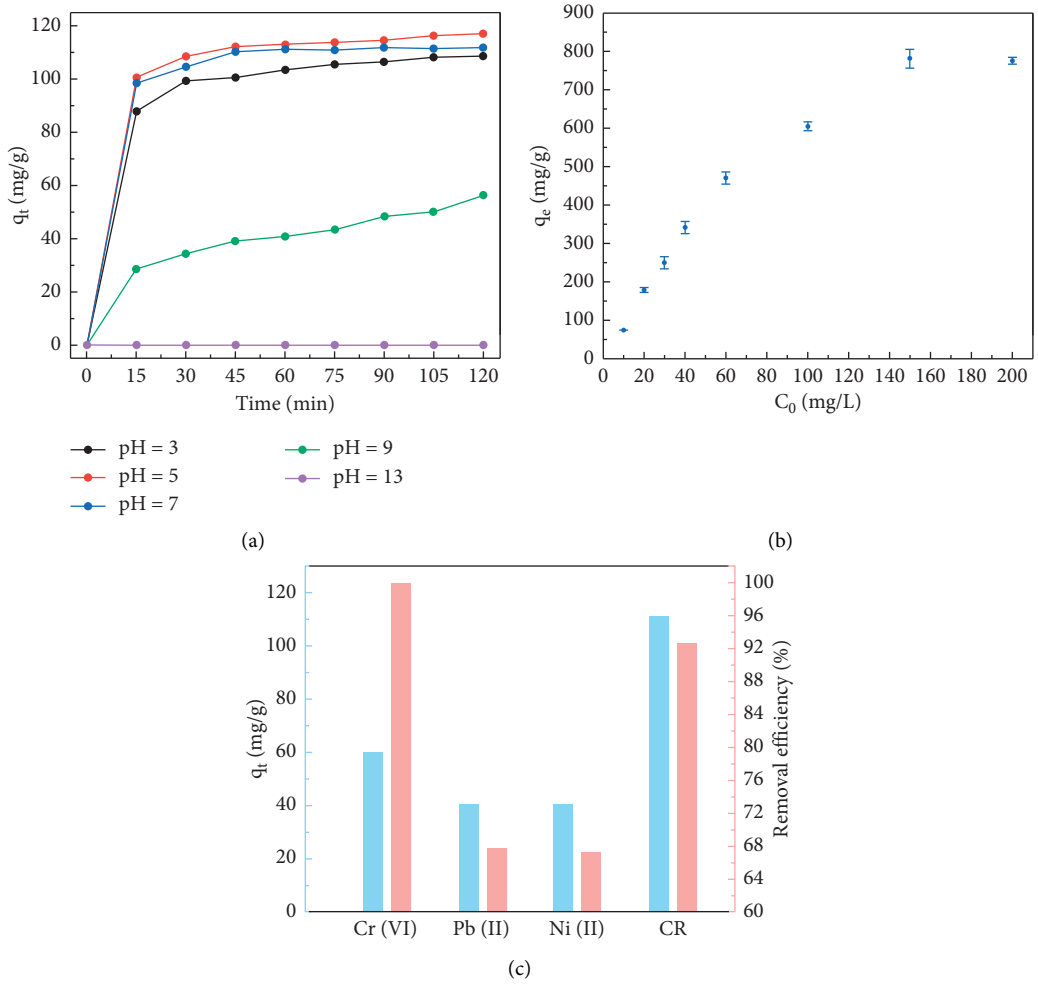

Figure 7: The effect of adsorption capacity for different (a) pH value (30 mg·L^{-1} dye, RT), (b) initial dye concentration (RT, pH = 7, t = 90 min), and (c) metal ion (30 mg·L^{-1} metal ion, RT, pH = 7, t = 2 h).

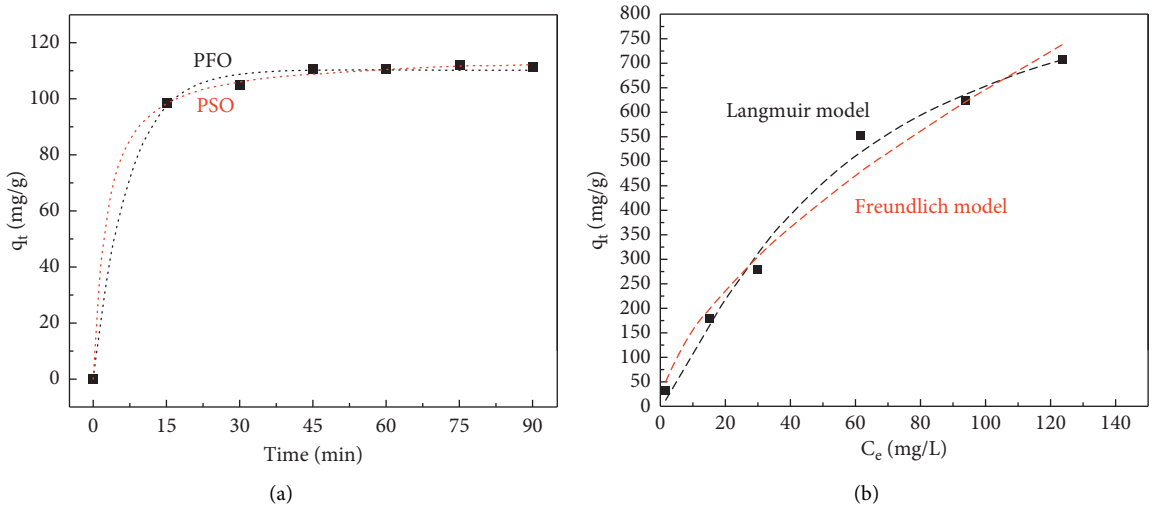

Figure 8: (a)Adsorption kinetics of CR onto GluP fitted by PFO and PSO models (0.25 g·L^{-1} adsorbent, 30 mg·L^{-1} dye, pH = 7, 25°C). (b) Adsorption isotherms of CR onto GluP fitted by Langmuir and Freundlich models (0.25 g·L^{-1} adsorbent, pH = 7, 25°C).

Table 2: Kinetic parameters for the adsorption of CR on GluP at 298 K.

Adsorbent	Pseudo-first-order model			Pseudo-second-order model		
	q_e (mg·g^{-1})	k_1 (min^{-1})	R^2	q_e (mg·g^{-1})	k_2 (g mg^{-1}·min^{-1})	R^2
GluP	110.35	0.14	0.99	115.41	0.14	0.99

Table 3: Langmuir and Freundlich isotherm fitting parameters at 298 K.

Adsorbent	Langmuir			Freundlich		
	K_L (L·mg^{-1})	q_m (mg·g^{-1})	R^2	n	K_F (mg$^{1-(1/n)}$ L$^{1/n}$g^{-1})	R^2
GluP	0.007	955.6	0.99	1.61	36.9	0.97

where C_e (mg·L^{-1}) is the equilibrium concentration of dye and q_m (mg·g^{-1}) is the maximum adsorption capacity. K_L (L·mg^{-1}) and K_F (mg$^{1-(1/n)}$·L$^{1/n}$g^{-1}) are constants for Langmuir and Freundlich models, respectively. All corresponding parameters are calculated by these two isotherms, and the results are listed in Table 3. As we can see, the correlation coefficient (R^2) of the Langmuir model (0.99) is better than that of the Freundlich model (0.97), and the value of n is less than 2, which suggests that the adsorption behavior of CR onto the as-synthesized GluP follows the Langmuir monolayer adsorption model [18, 24]. The theoretical maximum adsorption capacity calculated by equation (5) is 955.6 mg·g^{-1} with 0.25 g·L^{-1} adsorbent at 298 K. Therefore, the glutamate acid-doped polyaniline is a promising adsorbent for dye (especially Congo red) wastewater treatment. As shown in Table 4, the maximum adsorption capacity of different polyaniline-based adsorbents for Congo red was compared with the values from other reported results.

Moreover, the adsorption behavior of Congo red on GluP composites at different temperatures was also investigated for a better understanding of the adsorption process and the underlying mechanisms. Thus, three sets of adsorption experiments were carried out at three different temperatures (323, 333, and 343 K). The thermal parameters, for instance, the change of Gibbs free energy (ΔG), enthalpy (ΔH), and entropy (ΔS), were calculated by fitting the data to the following thermodynamic equations (7) and (8) [3]:

$$\Delta G = -RT \ln K, \tag{7}$$

$$\ln K = -\frac{\Delta H}{RT} + \frac{\Delta S}{R}, \tag{8}$$

where R is the universal gas constant (8.314 J·mol^{-1}·K^{-1}), T is the absolute temperature in Kelvin, and K represents the thermodynamic equilibrium constant (L·mol^{-1}). The corresponding thermodynamic parameters are presented in Table 5. As can be seen, the values of ΔG (kJ·mol^{-1}) were negative (−12.54, −14.93, and −17.80 kJ/mol at 323, 333, and 343 K, resp.) and decreased with increasing temperature in all tests. These results indicated that the adsorption process was favorable and spontaneous. Meanwhile, the values of ΔH and ΔS for GluP were 74.57 kJ·mol^{-1} and 0.27 kJ·mol^{-1}, which implies that the adsorption process for Congo red dye molecule was endothermic. This also reflects a good affinity between the adsorbent and the adsorbate during adsorption. Additionally, the positive value of ΔS also represents a good affinity between adsorbent (GluP composites) and adsorbate (Congo red) [3, 30].

Table 4: Comparison of the adsorption capacity of different adsorbents for Congo red.

Entry	Materials	Maximum adsorption capacity (mg/g)	References
1	PANI	250.01	[25]
2	GS/PANI/Fe_3O_4	248.12	[26]
3	*p*TSA-pani@GO-CNT	66.66	[27]
4	PANI@TiO2 PANI@SiO2	93 71	[28]
5	PANI-GO-Fe_3O_4	252.67	[29]
6	PNHM/MnO_2/Fe_3O_4	599.49	[30]
7	PANI nanotubes	955.6	This work

Table 5: Thermodynamic parameters for removal of Congo red by GluP (adsorbent: 0.25 g·L^{-1}; dye: 60 mg·L^{-1}; pH = 7; and volume: 20 mL).

Adsorbent	ΔG (kJ·mol^{-1})			ΔH (kJ·mol^{-1})	ΔS (kJ·mol^{-1}·K^{-1})
	323 K	333 K	343 K		
GluP	−12.54	−14.93	−17.80	74.57	0.27

3.4. Adsorption Mechanisms and Recyclability Study. In general, the main driving forces for the dye adsorption process are combined intermolecular interactions, including hydrogen bonding, π-π stacking interaction, and electrostatic attraction/repulsion. Therefore, the adsorption capacity is closely related to the chemical structure and external environment of adsorbent and adsorbate. If the electrostatic interaction dominates in Congo red dye molecule adsorption process in aqueous solution, the GluP composites will exhibit a lower adsorption capacity due to electrostatic repulsion between adsorbent and adsorbate at pH 3 because the amine and imine functional groups of polyaniline and Congo red are positively charged in such an acid environment. However, this speculation does not match the experimental data since the adsorption uptake of GluP composites was maintained at a fairly high level at pH = 3 (Figure 7(a)). On the other hand, intermolecular hydrogen

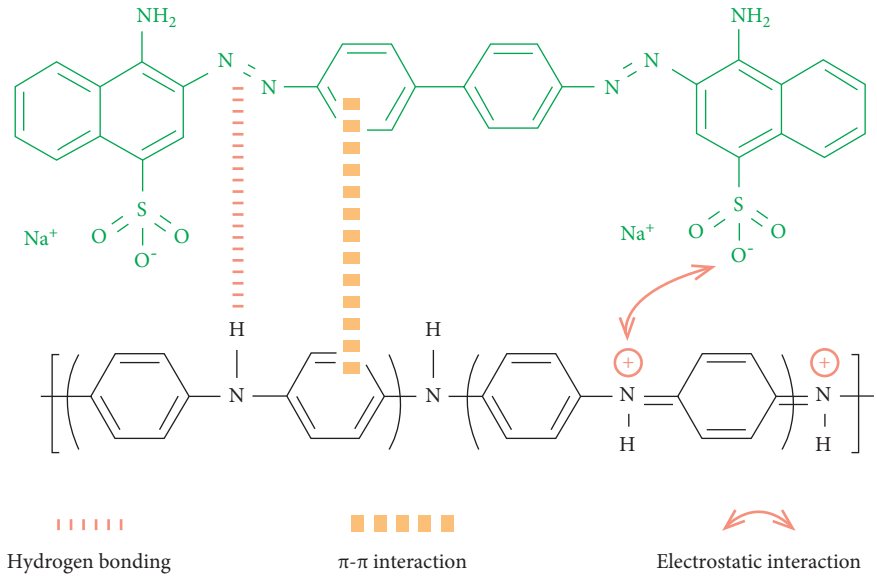

Figure 9: Plausible mechanism of Congo red adsorption by GluP composites.

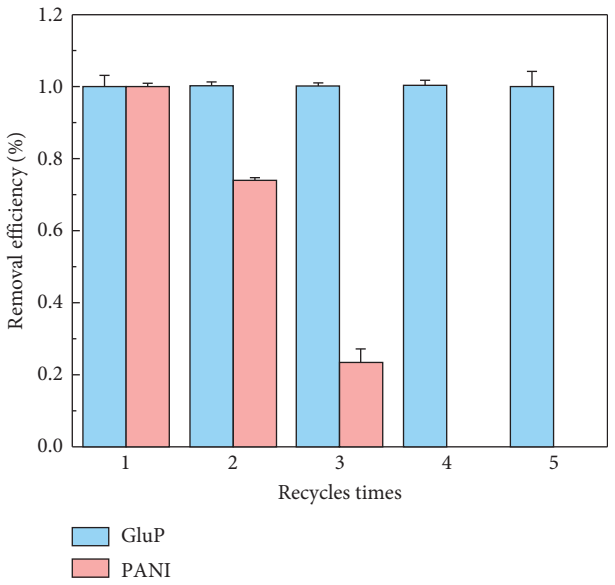

Figure 10: Recyclability study (0.5 g/L absorbent, 30 mg·L^{-1} dye, pH 7, RT, $t = 60$ min).

bonding of dye molecules usually results in multilayer adsorption [3], while the adsorption of Congo red follows the Langmuir monolayer adsorption model based on previous results (Table 3). This indicates that hydrogen bonding is not the dominant force for adsorption. According to the above analysis, the most likely driving force for Congo red is the π-π stacking interaction between benzene rings of polyaniline and dye molecules. Specifically, electrostatic attraction also plays an important role in dye adsorption, and hydrogen bonding will also be involved in dye-binding (Figure 9).

From a practical application point of view, the reusability of the adsorbent is an important indicator. After adsorption of the Congo red dyes, PANI and GluP composites were washed appropriately with dilute NaOH solution (1 M) and regenerated by washing with HCl solution (1 M) and rinsed with deionized water. Subsequently, the two adsorbents were recovered by centrifugation and dried in the oven overnight at 60°C. Then, the next round of the same adsorption experiments was repeated several times. The cycle stability of adsorbents was monitored and analyzed by UV-Vis absorption spectrometry, as shown in Figure 10. The results show that GluP still has a very high adsorption efficiency and no significant decrease was observed after five consecutive adsorption cycles. On the contrary, the removal efficiency of pure polyaniline nanomaterials (PANI) rapidly decreases to 74% after two repeated experiments. As the number of cycles further increases, the removal efficiency rapidly drops to zero (during the fourth cycle). This demonstrates that glutamic acid-doped polyaniline nanotubes (GluP) have much better cycle stability than pure polyaniline nanomaterials (PANI) and possess more promising applications.

4. Conclusions

In conclusion, we have successfully prepared an amino acid-doped polyaniline-based adsorbent material with a hollow tubular structure. In the adsorption experiments, the adsorbent presented a good dye removal capacity, as well as better adsorption efficiency for anionic dye molecules. The maximum adsorption capacity was around 117.0 mg·g^{-1} at pH 5. Besides, the GluP nanocomposites also have excellent adsorption capacity for metal ions, especially hexavalent chromium with an equilibrium adsorption capacity of 60.0 mg·g^{-1}. The adsorption kinetic behavior of GluP was in line with the pseudo-first-order model and Langmuir monolayer adsorption model for the dye Congo red at 298 K. In particular, the material did not significantly reduce the adsorption capacity after five reuses and showed good

recycling performance. Thus, this work not only offers a simple method to prepare polyaniline-based nanomaterials but also presents a promising adsorbent for organic dyes and heavy metal ions.

Data Availability

No data were used to support this study.

Conflicts of Interest

The authors declare that there are no conflicts of interest.

Authors' Contributions

Zhao Zhao and Yimin Yang contributed equally to this study.

Acknowledgments

This work was supported by the Scientific Research Project of Education Department of Hunan Province (no. 19C1907), Hunan Provincial Natural Science Foundation of China (no. 2021JJ41063), Hunan High-Level Talent Gathering Project Innovative Talents (no. 2019RS1061), the Research Startup Foundation of Central South University of Forestry and Technology (no. 2017YJ034), and Hunan Provincial Innovation Foundation for Postgraduate (no. CX20210866).

References

[1] Z. Salahshoor and A. Shahbazi, "Review of the use of mesoporous silicas for removing dye from textile wastewater," *European Journal of Environmental Sciences*, vol. 4, no. 2, pp. 116–130, 2014.

[2] N. P. Raval, P. U. Shah, and N. K. Shah, "Adsorptive amputation of hazardous azo dye congo red from wastewater: a critical review," *Environmental Science and Pollution Research*, vol. 23, no. 15, pp. 14810–14853, 2016.

[3] J. Shen, S. Shahid, I. Amura, A. Sarihan, M. Tian, and E. A. Emanuelsson, "Enhanced adsorption of cationic and anionic dyes from aqueous solutions by polyacid doped polyaniline," *Synthetic Metals*, vol. 245, pp. 151–159, 2018.

[4] A. K. Badawi, M. Abd Elkodous, and G. A. M. Ali, "Recent advances in dye and metal ion removal using efficient adsorbents and novel nano-based materials: an overview," *RSC Advances*, vol. 11, no. 58, pp. 36528–36553, 2021.

[5] Y. Fei and Y. H. Hu, "Design, synthesis, and performance of adsorbents for heavy metal removal from wastewater: a review," *Journal of Materials Chemistry*, vol. 10, no. 3, pp. 1047–1085, 2022.

[6] G. Ćirić-Marjanović, "Recent advances in polyaniline research: polymerization mechanisms, structural aspects, properties and applications," *Synthetic Metals*, vol. 177, no. 1, pp. 1–47, 2013.

[7] T. H. Qazi, R. Rai, and A. R. Boccaccini, "Tissue engineering of electrically responsive tissues using polyaniline based polymers: a review," *Biomaterials*, vol. 35, no. 33, pp. 9068–9086, 2014.

[8] F. Habtamu, S. Berhanu, and T. Mender, "Polyaniline supported Ag-doped ZnO nanocomposite: synthesis, characterization, and kinetics study for photocatalytic degradation of malachite green," *Journal of Chemistry*, vol. 2021, Article ID 2451836, 12 pages, 2021.

[9] A. Samadi, M. Xie, J. Li, H. Shon, C. Zheng, and S. Zhao, "Polyaniline-based adsorbents for aqueous pollutants removal: a review," *Chemical Engineering Journal*, vol. 418, no. 15, Article ID 129425, 2021.

[10] U. Rana, S. Mondal, J. Sannigrahi et al., "Aromatic bi-tri- and tetracarboxylic acid doped polyaniline nanotubes: effect on morphologies and electrical transport properties," *Journal of Materials Chemistry C*, vol. 2, no. 17, pp. 3382–3389, 2014.

[11] S. Bhadra, S. Chattopadhyay, N. K. Singha, and D. Khastgir, "Improvement of conductivity of electrochemically synthesized polyaniline," *Journal of Applied Polymer Science*, vol. 108, no. 1, pp. 57–64, 2008.

[12] L. Wang, X. L. Wu, W. H. Xu, X. J. Huang, J. H. Liu, and A. W. Xu, "Stable organic-inorganic hybrid of polyaniline/α-zirconium phosphate for efficient removal of organic pollutants in water environment," *ACS Applied Materials and Interfaces*, vol. 4, no. 5, pp. 2686–2692, 2012.

[13] U. Rana, K. Chakrabarti, and S. Malik, "Benzene tetracarboxylic acid doped polyaniline nanostructures: morphological, spectroscopic and electrical characterization," *Journal of Materials Chemistry*, vol. 22, no. 31, pp. 15665–15671, 2012.

[14] S. Shahabuddin, N. M. Sarih, F. H. Ismail, M. M. Shahid, and N. M. Huang, "Synthesis of chitosan grafted-polyaniline/Co_3O_4 nanotube nanocomposite and its photocatalytic activity toward methylene blue dye degradation," *RSC Advances*, vol. 5, no. 102, pp. 83857–83867, 2015.

[15] A. A. Farghali, M. Moussa, and M. H. Khedr, "Synthesis and characterization of novel conductive and magnetic nanocomposites," *Journal of Alloys and Compounds*, vol. 499, no. 1, pp. 98–103, 2010.

[16] X. Du, Y. Xu, L. Xiong, Y. Bai, J. Zhu, and S. Mao, "Polyaniline with high crystallinity degree: synthesis, structure, and electrochemical properties," *Journal of Applied Polymer Science*, vol. 131, no. 19, pp. 5829–5836, 2014.

[17] R. M. Khafagy, "Synthesis, characterization, magnetic and electrical properties of the novel conductive and magnetic polyaniline/$MgFe_2O_4$ nanocomposite having the core-shell structure," *Journal of Alloys and Compounds*, vol. 509, no. 41, pp. 9849–9857, 2011.

[18] V. Sharma, P. Rekha, and P. Mohanty, "Nanoporous hypercrosslinked polyaniline: an efficient adsorbent for the adsorptive removal of cationic and anionic dyes," *Journal of Molecular Liquids*, vol. 222, pp. 1091–1100, 2016.

[19] J. Shen, M. F. Evangelista, G. Mkongo et al., "Efficient defluoridation of water by monetite nanorods," *Adsorption*, vol. 24, no. 2, pp. 135–145, 2018.

[20] Q. Hu, C. Guo, D. Sun, Y. Ma, B. Qiu, and Z. Guo, "Extracellular polymeric substances induced porous polyaniline for enhanced Cr(VI) removal from wastewater," *ACS Sustainable Chemistry & Engineering*, vol. 5, no. 12, pp. 11788–11796, 2017.

[21] M. T. Yagub, T. K. Sen, S. Afroze, and H. Ang, "Dye and its removal from aqueous solution by adsorption: a review," *Advances in Colloid and Interface Science*, vol. 209, pp. 172–184, 2014.

[22] B. N. Patra and D. Majhi, "Removal of anionic dyes from water by potash alum doped polyaniline: investigation of kinetics and thermodynamic parameters of adsorption," *Journal of Physical Chemistry B*, vol. 119, no. 25, pp. 8154–8164, 2015.

[23] M. H. Mohamed, A. Dolatkhah, T. Aboumourad, L. Dehabadi, and L. D. Wilson, "Investigation of templated and supported polyaniline adsorbent materials," *RSC Advances*, vol. 5, no. 9, pp. 6976–6984, 2015.

[24] J. Xiao, Y. Tan, Y. Song, Q. Zheng, W. Lv, and Z. Xie, "Environmentally friendly reduced graphene oxide as a broad-spectrum adsorbent for anionic and cationic dyes via π-π interactions," *Journal of Materials Chemistry*, vol. 4, no. 31, pp. 12126–12135, 2016.

[25] H. Chafai, M. Laabd, S. Elbariji, M. Bazzaoui, and A. Albourine, "Study of congo red adsorption on the polyaniline and polypyrrole," *Journal of Dispersion Science and Technology*, vol. 38, no. 6, pp. 832–836, 2017.

[26] B. Mu, J. Tang, L. Zhang, and A. Wang, "Facile fabrication of superparamagnetic graphene/polyaniline/Fe_3O_4 nanocomposites for fast magnetic separation and efficient removal of dye," *Scientific Reports*, vol. 7, no. 1, p. 5347, 2017.

[27] M. O. Ansari, R. Kumar, S. A. Ansari, M. Barakat, A. Alshahrie, and M. H. Cho, "Anion selective pTSA doped polyaniline@graphene oxide-multiwalled carbon nanotube composite for Cr(VI) and congo red adsorption," *Journal of Colloid and Interface Science*, vol. 496, pp. 407–415, 2017.

[28] M. Maruthapandi, L. Eswaran, J. H. Luong, and A. Gedanken, "Sonochemical preparation of polyaniline@TiO_2 and polyaniline@SiO_2 for the removal of anionic and cationic dyes," *Ultrasonics Sonochemistry*, vol. 62, Article ID 104864, 2020.

[29] C. Lv, J. Zhang, G. Li, H. Xi, M. Ge, and T. Goto, "Facile fabrication of self-assembled lamellar PANI-GO-Fe_3O_4 hybrid nanocomposites with enhanced adsorption capacities and easy recyclicity towards ionic dyes," *Colloids and Surfaces A: Physicochemical and Engineering Aspects*, vol. 585, Article ID 124147, 2020.

[30] S. Dutta, S. K. Srivastava, B. Gupta, and A. K. Gupta, "Hollow polyaniline microsphere/MnO_2/Fe_3O_4 nanocomposites in adsorptive removal of toxic dyes from contaminated water," *ACS Applied Materials & Interfaces*, vol. 13, no. 45, pp. 54324–54338, 2021.